




# The milling effect on nickel ferrite particles studied using magnetization measurements and Mössbauer spectroscopy

M. V. Ushakov<sup>1</sup> · M. I. Oshtrakh<sup>1</sup>  · A. V. Chukin<sup>1</sup> ·  
V. Šepelák<sup>2,3</sup> · I. Felner<sup>4</sup> · V. A. Semionkin<sup>1</sup>

© Springer International Publishing AG, part of Springer Nature 2017

**Abstract** Samples of  $\text{NiFe}_2\text{O}_4$  nanoparticles N1 (nonactivated), N2 (milled for 15 min) and N3 (milled for 30 min) were studied using X-ray diffraction, scanning electron microscopy with energy dispersion spectroscopy, isothermal magnetization measurement and Mössbauer spectroscopy with respect to analyze the effect of particle milling on their magnetic properties. It was shown that an increase of the milling time lead to: (i) a decrease of particles' size, (ii) a decrease of the saturation magnetic moment and (iii) an appearance of paramagnetic doublet in the Mössbauer spectra of  $\text{NiFe}_2\text{O}_4$  nanoparticles.

**Keywords** Mössbauer spectroscopy · Magnetic measurements ·  $\text{NiFe}_2\text{O}_4$  nanoparticles · Milling effect · Hyperfine parameters

---

This article is part of the Topical Collection on *Proceedings of the International Conference on the Applications of the Mössbauer Effect (ICAME 2017), Saint-Petersburg, Russia, 3–8 September 2017*  
Edited by Valentin Semenov

---

✉ M. I. Oshtrakh  
oshtrakh@gmail.com

<sup>1</sup> Institute of Physics and Technology, Ural Federal University, Ekaterinburg, 620002, Russian Federation

<sup>2</sup> Institute of Nanotechnology, Karlsruhe Institute of Technology, Hermann-von-Helmholtz-Platz 1, 76344 Eggenstein-Leopoldshafen, Germany

<sup>3</sup> Institute of Physics, Faculty of Mining and Geology, VŠB-Technical University of Ostrava, 70833 Ostrava, Czech Republic

<sup>4</sup> Racah Institute of Physics, The Hebrew University, Jerusalem, 91904 Israel

## 1 Introduction

Nickel ferrites nanoparticles are widely used in different domains of technical applications, i.e. in magnetic storage devices, in new electronics (spintronics), in magnetic resonance, Li-ion batteries and supercapacitors and others [1–8]. Therefore, nanoparticles structure and magnetic properties are keys to their usage in these domains. It is known that nanoparticle synthesis route influenced on nanoparticle's size and size distribution [9–11], structural and magnetic properties [12–14]. Ball milling appears quite simple and effective method for nanoparticles synthesis.

Mössbauer spectroscopy is one of the useful techniques for the study of structure and magnetic properties of iron containing nanoparticles [15–19]. Typically the Mössbauer spectrum of  $\text{NiFe}_2\text{O}_4$  nanoparticles consists of two magnetic sextets related to the  $^{57}\text{Fe}$  nuclei in tetrahedral (A) and octahedral (B) sites of inverse spinel. However, it was shown that there is a variation of the number of  $\text{Ni}^{2+}$  ions in the local microenvironment of  $\text{Fe}^{3+}$  in both the A and B positions. Therefore, the high precision Mössbauer spectra of  $\text{NiFe}_2\text{O}_4$  nanoparticles measured with a higher order of discretization of the velocity reference signal (the high velocity resolution Mössbauer spectroscopy) demonstrated more complex spectra than those measured using conventional Mössbauer spectrometers [20–23]. In the present work we continue the above mentioned study of  $\text{NiFe}_2\text{O}_4$  nanoparticles in order to analyze the effect of ball milling on the  $^{57}\text{Fe}$  hyperfine parameters using Mössbauer spectroscopy.

## 2 Experimental

Polycrystalline  $\text{NiFe}_2\text{O}_4$  was prepared by the conventional ceramic method (further referred to as the nonactivated sample N1). The nonactivated sample (2 g) was ground for various times (15 min and 30 min) in a planetary ball mill EI 2 × 150 at the Institute of Solid State Chemistry (Novosibirsk, Russian Federation) at room temperature. The ceramic-covered grinding chamber (150 cm<sup>3</sup> in volume) and balls made of  $\alpha\text{-Al}_2\text{O}_3$  with diameter of 3 to 5 mm were used. The ball-to-powder weight ratio was 50:1. Grinding experiments were performed in air at 750 rpm. The milled samples of  $\text{NiFe}_2\text{O}_4$  nanoparticles were marked as N2 and N3 for 15 and 30 min milling, respectively. Nanoparticle sample powders were used for characterization using several techniques. Samples for Mössbauer spectroscopy were glued on iron free Al foil. Thickness of these samples was less than 8 mg Fe/cm<sup>2</sup>.

The three samples of  $\text{NiFe}_2\text{O}_4$  nanoparticles were characterized by X-ray diffraction (XRD), scanning electron microscopy (SEM) with energy dispersion spectroscopy (EDS) and magnetization measurements. XRD patterns were measured using Shimadzu diffractometer in scanning range 15–132° with degree step of 0.05° per 10 s. SEM images with EDS were obtained using scanning electron microscope SIGMA VP (Carl Zeiss) with an X-max 80 energy dispersive spectroscopy device (Oxford Instruments). Magnetization measurements on  $\text{NiFe}_2\text{O}_4$  samples mounted in gel-caps have been performed using a Quantum Design SQUID magnetometer at various applied magnetic fields (H) at 295 K at the Racah Institute of Physics (the Hebrew University, Jerusalem, Israel).

Mössbauer spectra were measured using an automated precision Mössbauer spectrometric system built on the base of the SM-2201 spectrometer with a saw-tooth shape velocity reference signal formed by the digital-analog converter using discretization of  $2^{12}$  (quantification using 4096 steps) at the Institute of Physics and Technology, Ural Federal University (Ekaterinburg, Russian Federation). Details and characteristics of this set up are given

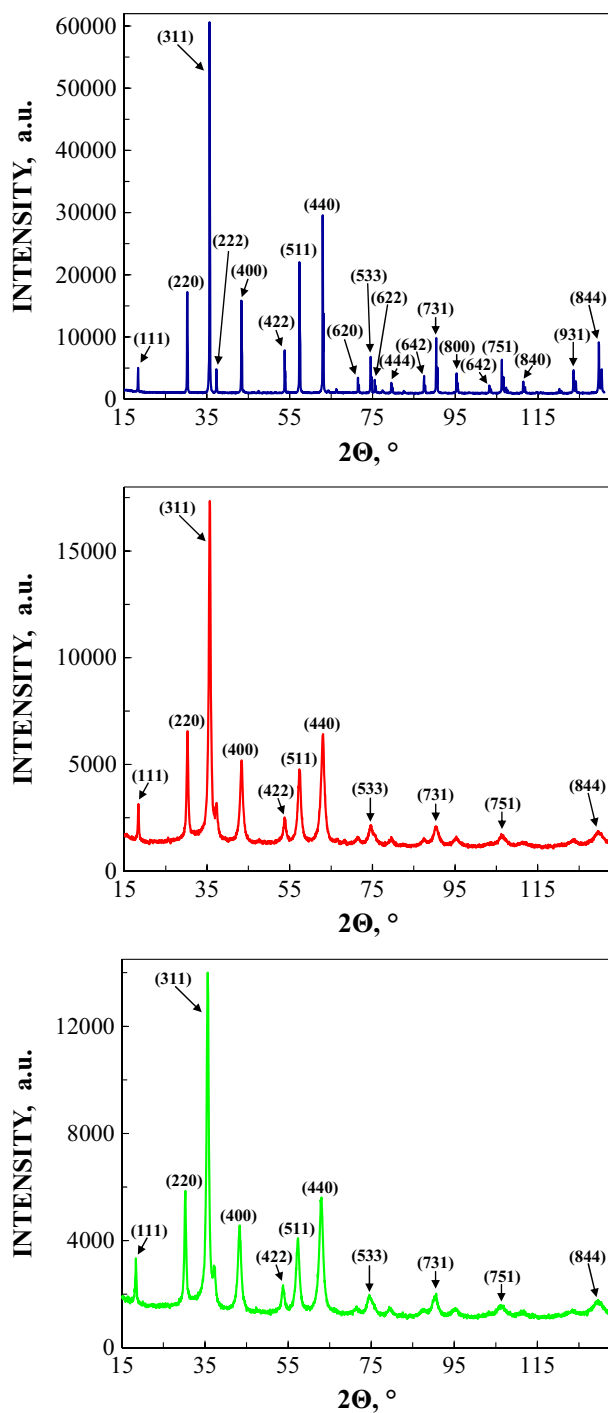


**Fig. 1** X-ray diffraction patterns for  $\text{NiFe}_2\text{O}_4$  samples: N1 (nonactivated), N2 (milled for 15 min) and N3 (milled for 30 min)

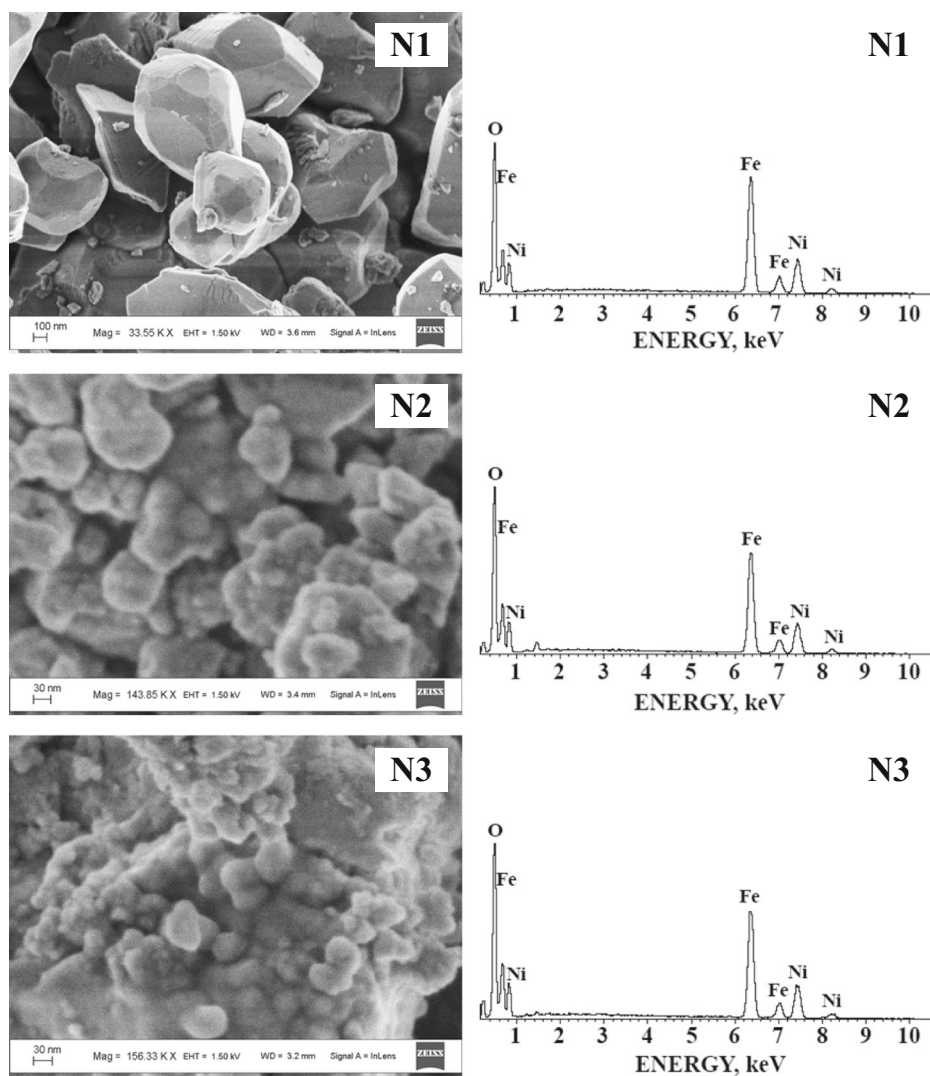


**Fig. 2** Scanning electron microscopy images (left panel) and energy dispersion spectra (right panel) for  $\text{NiFe}_2\text{O}_4$  samples: N1 (nonactivated), N2 (milled for 15 min) and N3 (milled for 30 min)

**Table 1** Chemical composition of  $\text{NiFe}_2\text{O}_4$  samples N1, N2 and N3 obtained using EDS

Sample	Element content, at. %		
	O	Fe	Ni
N1	54.86	31.27	13.86
N2	60.07	27.39	12.53
N3	59.87	27.57	12.57

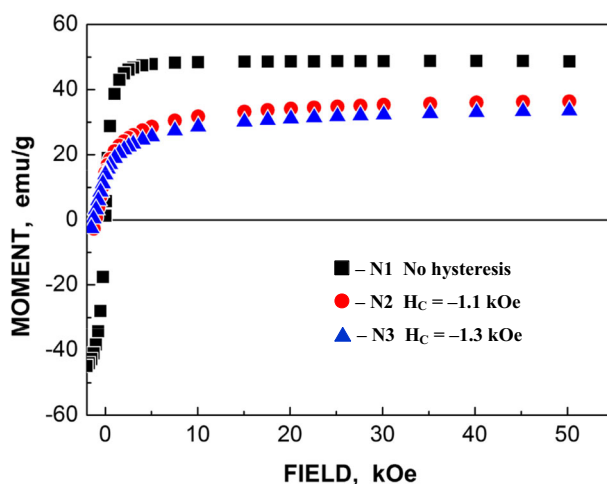


**Fig. 3** Room temperature isothermal magnetization curves for  $\text{NiFe}_2\text{O}_4$  samples: N1 (nonactivated), N2 (milled for 15 min) and N3 (milled for 30 min);  $H_C$  is coercive force

elsewhere [24–27]. The  $1.8 \times 10^9$  Bq  $^{57}\text{Co}(\text{Rh})$  source (Ritverc GmbH, St. Petersburg) was at room temperature. The Mössbauer spectra were measured in transmission geometry with moving absorber at 295 K and recorded in 4096 channels. Then the spectra were converted into 1024 channels to increase signal-to-noise ratio. Statistics in the converted Mössbauer spectra of  $\text{NiFe}_2\text{O}_4$  samples was in the range  $\sim(1.1\text{--}1.3) \times 10^6$  counts per channel and signal-to-noise ratio for these spectra was in the range 36–59.

The Mössbauer spectra of  $\text{NiFe}_2\text{O}_4$  were computer fitted with the least squares procedure using UNIVEM-MS program with a Lorentzian line shape. The spectral parameters such as: isomer shift,  $\delta$ , quadrupole splitting (quadrupole shift  $\varepsilon$  for magnetically split spectra),  $\Delta E_Q = 2\varepsilon$ , magnetic hyperfine field,  $H_{\text{eff}}$ , line width,  $\Gamma$ , relative subspectrum area,  $A$ , and statistical quality of the fit,  $\chi^2$ , were determined. An instrumental (systematic) error for each spectrum point was  $\pm 0.5$  channel (the velocity scale), the instrumental (systematic) error for the hyperfine parameters was  $\pm 1$  channel. If an error calculated with the fitting procedure (fitting error) for these parameters exceeded the instrumental (systematic) error we used the larger error instead. Criteria for the best fit were differential spectrum,  $\chi^2$  value and a physical meaning of the spectral parameters. Values of  $\delta$  are given relative to  $\alpha\text{-Fe}$  at 295 K. The Mössbauer spectrum of standard absorber  $\alpha\text{-Fe}$  foil (7  $\mu\text{m}$ ) demonstrated Lorentzian line shape with the values of  $\Gamma_{1,6} = 0.242 \pm 0.012$  mm/s,  $\Gamma_{2,5} = 0.238 \pm 0.012$  mm/s and  $\Gamma_{3,4} = 0.232 \pm 0.012$  mm/s (4096 channels).

### 3 Results and discussion

X-ray diffraction patterns of the samples N1, N2 and N3 are shown in Fig. 1. The obtained reflexes correspond to nickel ferrite crystals mainly. The presence of two weak peaks at  $2\theta$  of  $44^\circ$  and  $64^\circ$  indicates probably a small metal contamination. Lattice parameters for these samples were:  $a = 8.337(4)$  Å (N1),  $a = 8.342(4)$  Å (N2) and  $a = 8.344(5)$  Å (N3).

**Fig. 4** Mössbauer spectra of  $\text{NiFe}_2\text{O}_4$  samples N1 (nonactivated), N2 (milled for 15 min) and N3 (milled for 30 min) measured at 295 K. Indicated components are the results of the best fits (A1–A5 and B1–B5 are the magnetic sextets related to the A and B sites, respectively; S1–S8 are magnetic sextets, D1 is a paramagnetic doublet parameters of which are collected in Table 2). Differential spectra are shown below. Inserts in the top spectrum demonstrate misfits for outer sextet peaks for the fit using one sextet for both A and B sites, respectively

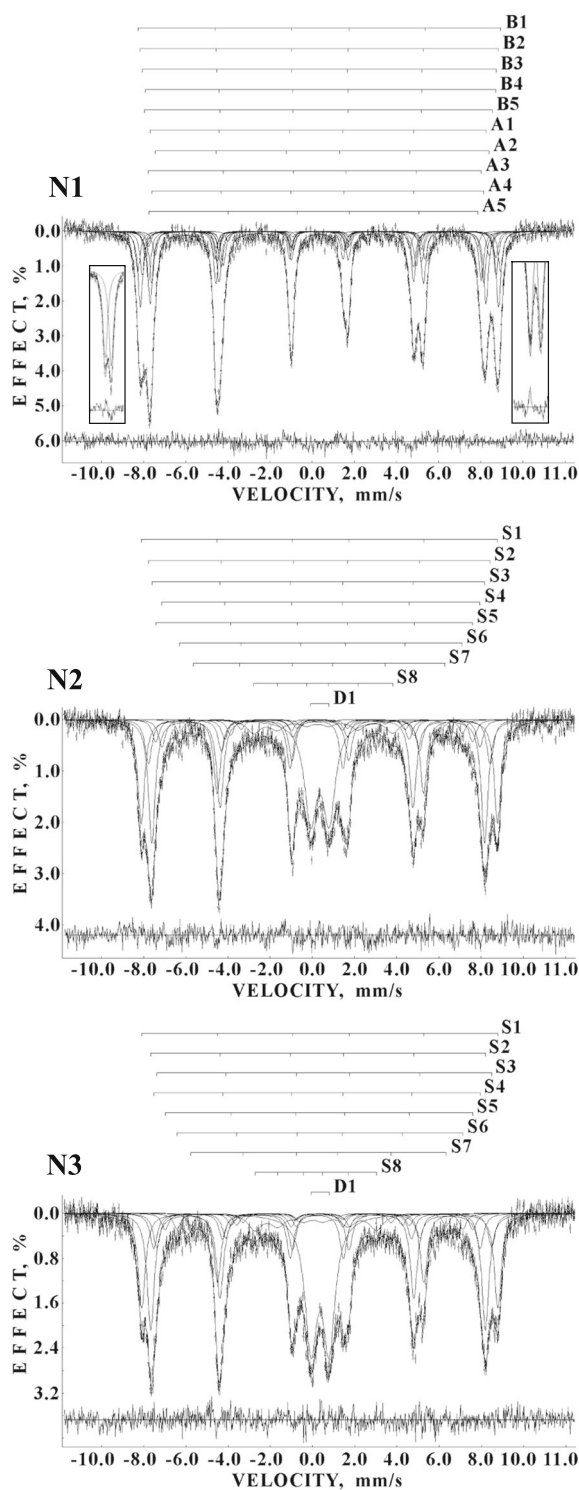


**Table 2** Mössbauer parameters for NiFe<sub>2</sub>O<sub>4</sub> particles: samples: N1 (nonactivated), N2 (milled for 15 min) and N3 (milled for 30 min)

Sample	$\Gamma$ , mm/s	$\delta$ , mm/s	$\Delta E_Q/2\varepsilon$ , mm/s	$H_{\text{eff}}$ , kOe	A, %	Fe site <sup>a</sup>
N1	$0.265 \pm 0.048$	$0.355 \pm 0.024$	$-0.383 \pm 0.024$	$534.4 \pm 0.8$	9.75	B1
	$0.265 \pm 0.048$	$0.354 \pm 0.024$	$-0.015 \pm 0.024$	$527.4 \pm 0.8$	18.38	B2
	$0.265 \pm 0.048$	$0.335 \pm 0.024$	$-0.001 \pm 0.017$	$520.8 \pm 1.0$	10.56	B3
	$0.265 \pm 0.048$	$0.393 \pm 0.025$	$0.019 \pm 0.042$	$515.8 \pm 1.8$	6.33	B4
	$0.265 \pm 0.048$	$0.348 \pm 0.027$	$-0.091 \pm 0.057$	$512.3 \pm 1.6$	3.48	B5
	$0.265 \pm 0.048$	$0.242 \pm 0.024$	$0.080 \pm 0.024$	$494.4 \pm 0.8$	17.57	A1
	$0.265 \pm 0.048$	$0.253 \pm 0.024$	$0.440 \pm 0.019$	$491.9 \pm 0.8$	5.88	A2
	$0.265 \pm 0.048$	$0.245 \pm 0.024$	$-0.230 \pm 0.024$	$490.0 \pm 0.8$	11.98	A3
	$0.265 \pm 0.048$	$0.257 \pm 0.024$	$0.015 \pm 0.024$	$488.9 \pm 0.8$	12.47	A4
	$0.265 \pm 0.048$	$0.289 \pm 0.024$	$-0.480 \pm 0.036$	$484.2 \pm 1.5$	3.60	A5
N2	$0.387 \pm 0.048$	$0.358 \pm 0.024$	$-0.047 \pm 0.024$	$524.4 \pm 0.8$	23.04	S1
	$0.387 \pm 0.048$	$0.356 \pm 0.024$	$-0.054 \pm 0.024$	$502.8 \pm 0.8$	9.84	S2
	$0.387 \pm 0.048$	$0.239 \pm 0.024$	$0.083 \pm 0.024$	$489.8 \pm 0.8$	27.39	S3
	$0.387 \pm 0.048$	$0.311 \pm 0.024$	$0.190 \pm 0.024$	$468.0 \pm 1.0$	6.12	S4
	$0.387 \pm 0.048$	$0.280 \pm 0.024$	$-0.387 \pm 0.027$	$466.3 \pm 1.1$	4.97	S5
	$0.387 \pm 0.048$	$0.454 \pm 0.024$	$-0.097 \pm 0.030$	$416.1 \pm 1.1$	3.10	S6
	$0.387 \pm 0.048$	$0.158 \pm 0.034$	$0.323 \pm 0.069$	$369.8 \pm 2.3$	1.39	S7
	$0.776 \pm 0.070$	$0.376 \pm 0.027$	$0.272 \pm 0.045$	$204.9 \pm 1.7$	5.85	S8
	$0.705 \pm 0.048$	$0.356 \pm 0.024$	$0.876 \pm 0.024$	—	18.31	D1
N3	$0.406 \pm 0.048$	$0.363 \pm 0.024$	$-0.041 \pm 0.024$	$523.7 \pm 0.8$	20.66	S1
	$0.406 \pm 0.048$	$0.519 \pm 0.024$	$0.063 \pm 0.024$	$492.4 \pm 0.8$	7.39	S2
	$0.406 \pm 0.048$	$0.232 \pm 0.024$	$0.055 \pm 0.024$	$492.1 \pm 0.8$	25.40	S3
	$0.406 \pm 0.048$	$0.208 \pm 0.024$	$-0.009 \pm 0.024$	$479.8 \pm 1.0$	7.68	S4
	$0.406 \pm 0.048$	$0.333 \pm 0.024$	$-0.058 \pm 0.030$	$452.4 \pm 1.4$	3.56	S5
	$0.406 \pm 0.048$	$0.338 \pm 0.024$	$0.018 \pm 0.028$	$420.4 \pm 1.1$	3.48	S6
	$0.406 \pm 0.048$	$0.241 \pm 0.024$	$0.068 \pm 0.035$	$375.7 \pm 1.3$	2.79	S7
	$0.776 \pm 0.048$	$0.083 \pm 0.025$	$0.137 \pm 0.040$	$178.8 \pm 1.6$	6.72	S8
	$0.686 \pm 0.048$	$0.352 \pm 0.024$	$0.861 \pm 0.024$	—	22.31	D1

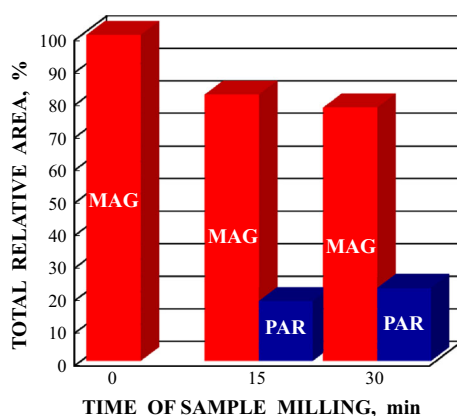
<sup>a</sup>Indicated Fe sites correspond to Mössbauer spectra components shown in Fig. 4

Crystallite sizes, estimated using Scherer formula, were as follows: 150, 28 and 25 nm for the samples N1, N2 and N3, respectively.

Selected scanning electron microscopy images with energy dispersion spectra for NiFe<sub>2</sub>O<sub>4</sub> samples N1, N2 and N3 are shown in Fig. 2.

SEM images demonstrate also a decrease in the particle sizes for milled samples in agreement with XRD data. Chemical analysis using EDS showed small variations in chemical composition of the samples N1, N2 and N3 as can be seen from Table 1. According to Table 1, there is a deviation from NiFe<sub>2</sub>O<sub>4</sub> stoichiometry (57 at.% O, 29 at.% Fe and 14 at.% Ni) which is slightly varied for nonactivated and milled samples.

**Fig. 5** The change of the total relative area of magnetic (MAG)/paramagnetic (PAR) components in the Mössbauer spectra of  $\text{NiFe}_2\text{O}_4$  samples N1, N2 and N2 with increase of milling time



Room temperature isothermal magnetization curves measured for N1, N2 and N3  $\text{NiFe}_2\text{O}_4$  samples are shown in Fig. 3. These results demonstrated that the saturation magnetic moment ( $M_S$ ) decreases for the milled samples due to a decrease in particle's size and probably due to appearance of small paramagnetic component. Hysteresis loops appear for samples N2 and N3 only and the coercive force ( $H_C$ ) increases with increasing the milling time. Therefore, milling influences the magnetic hardness of nickel ferrite particles due to size decreasing. Moreover, within the uncertainty value (0.1 kOe), both N2 and N3 samples exhibit similar  $H_C$  values because of their slightly different particles size.

Mössbauer spectra of  $\text{NiFe}_2\text{O}_4$  samples N1, N2 and N3 measured at 295 K are shown in Fig. 4. The spectrum of nonactivated  $\text{NiFe}_2\text{O}_4$  particles (N1) with a larger size (150 nm) demonstrates the shape of two six-line patterns similar to other  $\text{NiFe}_2\text{O}_4$  bulk samples or particles with a size larger than 20 nm (see, for instance, [28–31]). However, the fit of this Mössbauer spectrum using two magnetic sextets related to the A and B sites in  $\text{NiFe}_2\text{O}_4$  appeared to be not good as shown in Fig. 4: see misfits in insets for the spectrum of N1 sample. These misfits indicate that two magnetic sextets are not enough for a good spectrum fit. Basing on our recent study of  $\text{NiFe}_2\text{O}_4$  nanoparticles with average sizes of 25 and 35 nm using the estimation of different numbers of  $\text{Ni}^{2+}$  cations in the local microenvironment of the  $^{57}\text{Fe}$  nuclei in both A and B sites [20–23], we used the same model (a superposition of 10 magnetic sextets with the same line width with a free variation) to fit the Mössbauer spectrum of  $\text{NiFe}_2\text{O}_4$  sample N1. The result of this fit demonstrates significant improvement of the differential spectrum (see Fig. 4, N1) and decrease in the values of  $\chi^2$  from 2.873 down to 2.196 (the value of  $\sigma$ , the standard deviation for  $\chi^2$  for the 1024-channel spectra, is 0.044 [26]). Mössbauer parameters of spectral components are given in Table 2. On the basis of these parameters 5 sextets can be related to the  $^{57}\text{Fe}$  in the A sites (A1–A5) while other 5 sextets can be associated with the  $^{57}\text{Fe}$  in the B sites (B1–B5) in agreement with our previous result [23]. In contrast, the Mössbauer spectra of milled samples N2 and N3 consist of magnetic sextets and paramagnetic doublet (see Fig. 4). These spectra we cannot fit using above mentioned model. The most appropriate fits for the spectra of samples N2 and N3 were carried out using 7 magnetic sextets with the same line width varied during the fit, 1 magnetic sextet with free variation of the line width and one quadrupole doublet with free variation of parameters. The results of these fits are shown in Fig. 4 for N2 and N3 samples and Mössbauer parameters are given in Table 2. In the latter case we were unable to relate magnetic sextets S1–S8 to the possible iron sites in nickel ferrite. Moreover, sextet S8 looks



like collapsing sextet with smaller  $H_{\text{eff}}$  and broad line width. This sextet indicates a slow-down of magnetic relaxation due to a size decreasing. Observation of a quadrupole doublet in these spectra showed the presence of small  $\text{NiFe}_2\text{O}_4$  nanoparticles in the superparamagnetic state. Figure 5 demonstrates the change of the ratio of magnetic/paramagnetic states in  $\text{NiFe}_2\text{O}_4$  samples N1, N2 and N3 as a result of milling.

## 4 Conclusion

Study of  $\text{NiFe}_2\text{O}_4$  samples: N1 (nonactivated), N2 (milled for 15 min) and N3 (milled for 30 min) using X-ray diffraction, scanning electron microscopy with energy dispersion spectroscopy, magnetization measurements and Mössbauer spectroscopy demonstrated the effect of milling on the particle size and magnetic properties. The saturation magnetic moment decreases while hysteresis loops appear and the coercive force increases for samples N2 and N3 only with increasing the milling time. The Mössbauer spectra demonstrated significant changes for the milled samples N2 and N3 in comparison with nonactivated sample N1. Doublets D1 appeared in the N2 and N3 Mössbauer spectra are related to the small paramagnetic nanoparticles with the fast magnetic moment relaxation. Parameters of some spectral components obtained for the N2 and N3 samples could not be explained yet and required a further study. However, a large number of components could be a result of different numbers of  $\text{Ni}^{2+}$  in the local microenvironment of the  $^{57}\text{Fe}$  in the A and B sites in nickel ferrite and nanoparticles' size distribution.

**Acknowledgements** This work was supported by the Ministry of Education and Science of the Russian Federation (the Project # 3.1959.2017/4.6) and by the Act 211 Government of the Russian Federation, contract No. 02.A03.21.0006.

## References

1. Zhao, H., Zheng, Z., Wong, K.W., Wang, S., Huang, B., Li, D.: *Electrochem. Commun.* **9**, 2606–2610 (2007)
2. Karaagac, O., Atmara, S., Kockar, H.: *J. Supercond. Nov. Magn.* **30**, 2359–2369 (2017)
3. Islam, M., Ali, G., Jeong, M.-J., Choi, W., Chung, K.Y., Jung, H.-G.: *ACS Appl. Mat. Interface* **9**, 14833–14843 (2017)
4. Deshmukh, S.S., Humbe, A.V., Kumar, A., Dorik, R.G., Jadhav, K.M.: *J. Alloys Compd.* **704**, 227–236 (2017)
5. Virumblares, M., Saez-Puche, R., Blanco-Gutierrez, V., Torraivo-Fernandez, M.J.: *J. Phys. Chem. C* **121**, 4029–4036 (2017)
6. El-Sayed, K., Mohamed, M.B., Hamdy, S., Ata-Allah, S.S.: *J. Mag. Mag. Mat.* **423**, 291–300 (2017)
7. Kesavamoorthi, R., Raja, C.R.: *J. Supercond. Nov. Magn.* **29**, 2729–2735 (2016)
8. Kumari, V., Dey, K., Giri, S., Bhaumik, A.: *RCS Adv.* **6**, 45701–45707 (2016)
9. He, Y.J., Pang, X.C., Jiang, B.B., Feng, C.W., Harn, Y.W., et al.: *Angew. Chem. Int. Ed.* **56**, 12946–12951 (2017)
10. Konkgaew, T., Sakurai, K.: *Chem. Lett.* **46**, 1493–1496 (2017)
11. Teixeira, D., Quesada-Cabrera, R., Powell, M.J., Goh, G.K.L., Sankar, G., Parkin, I.P., Palgrave R.G.: *New J. Chem.* **41**, 9216–9222 (2017)
12. Hussein, S.I., Elkady, A.S., Rashad, M.M., Mostafa, A.G., Megahid, R.M.: *J. Magn. Magn. Mater.* **379**, 9–15 (2015)
13. Li, J., Li, J., Chen, L., Lin, Y.Q., Liu, X., Gong, X., Li, D.: *J. Magn. Magn. Mater.* **374**, 157–163 (2015)
14. Esir, S., Baykal, A., Sozeri, H.: *J. Supercond. Nov. Magn.* **27**, 1309–1314 (2014)
15. Siddique, M., Butt, N.M.: *Physica B* **405**, 4211–4215 (2010)
16. Thakur, M., De, K., Giri, S., Si, S., Kotal, A., Mandal, T.K.: *J. Phys. Condens. Matter* **18**, 9093–9104 (2006)

17. Kalska, B., Paggel, J.J., Fumagal, P., Rybczynski, J., Satula, D., Hilgendorff, M., Giersig, M.: *J. Appl. Phys.* **95**, 1343–1350 (2004)
18. Zheng, H., Yang, Y., Zhou, M., Li, F.: *Hyperfine Interact.* **189**, 131–136 (2009)
19. Compeán-Jasso, M.E., Ruiz, F., Martínez, J.R., Herrera-Gómez, A.: *Mater. Lett.* **62**, 4248–4250 (2008)
20. Oshtrakh, M.I., Ushakov, M.V., Senthilkumar, B., Selvan, R.K., Sanjeeviraja, C., Semionkin, V.A.: *AIP Conference Proceedings*, vol. 1489, pp. 115–122. AIP Publishing, Melville (2012)
21. Oshtrakh, M.I., Ushakov, M.V., Senthilkumar, B., Selvan, R.K., Sanjeeviraja, C., Felner, I., Semionkin, V.A.: *Hyperfine Interact.* **219**, 7–12 (2013)
22. Ushakov, M.V., Oshtrakh, M.I., Felner, I., Semenova, A.S., Kellerman, D.G., Šepelák, V., Semionkin, V.A., Morais, P.C.: *J. Magn. Magn. Mater.* **431**, 46–48 (2017)
23. Ushakov, M.V., Senthilkumar, B., Kalai Selvan, R., Felner, I., Oshtrakh, M.I.: *Mat. Chem. Phys.* **202**, 159–168 (2017)
24. Oshtrakh, M.I., Semionkin, V.A., Milder, O.B., Novikov, E.G.: *J. Radioanal. Nucl. Chem.* **281**, 63–67 (2009)
25. Semionkin, V.A., Oshtrakh, M.I., Milder, O.B., Novikov, E.G.: *Bull. Russ. Acad. Sci.: Phys.* **74**, 416–420 (2010)
26. Oshtrakh, M.I., Semionkin, V.A.: *Spectrochim. Acta A Mol. Biomol. Spectrosc.* **100**, 78–87 (2013)
27. Oshtrakh, M.I., Semionkin, V.A.: *AIP Conference Proceedings*, vol. 1781, 020019. AIP Publishing, Melville (2016)
28. Ahlawat, A., Sathe, V.G., Reddy, V.R., Gupta, A.: *J. Magn. Magn. Mater.* **323**, 2049–2054 (2011)
29. Šepelák, V., Bergmann, I., Feldhoff, A., Heitjans, P., Krumeich, F., Menzel, D., Litterst, F.J., Campbell, S.J., Becker, K.D.: *J. Phys. Chem. C* **111**, 5026–5033 (2007)
30. Ramalho, M.A.F., Gama, L., Antonio, S.G., Paiva-Santos, C.O., Miola, E.J., Kiminami, R.H.G.A., Costa A.C.F.M.: *J. Mater. Sci.* **42**, 3603–3606 (2007)
31. Mahmoud, M.H., Elshahawy, A.M., Makhoulouf, S.A., Hamdeh, H.H.: *J. Magn. Magn. Mater.* **343**, 21–26 (2013)